Biogeosciences Discuss., 12, 6405–6443, 2015
www.biogeosciences-discuss.net/12/6405/2015/
doi:10.5194/bgd-12-6405-2015

Biogeosciences Discussions
Open Access

Coupling the chemical dynamics of carbonate and dissolved inorganic nitrogen systems in the eutrophic and turbid inner Changjiang (Yangtze River) Estuary

W.-D. Zhai[1,2] **and X.-L. Yan**[3]

[1]State Key Laboratory of Marine Environmental Science, Xiamen University, Xiamen 361102, China
[2]National Marine Environmental Monitoring Center, Dalian 116023, China
[3]College of Ocean and Earth Sciences, Xiamen University, Xiamen 361102, China

Received: 3 March 2015 – Accepted: 13 April 2015 – Published: 30 April 2015

Correspondence to: W.-D. Zhai (wdzhai@126.com)

Published by Copernicus Publications on behalf of the European Geosciences Union.

Abstract

To better understand biogeochemical processes controlling CO_2 dynamics in those eutrophic large-river estuaries and coastal lagoons, we investigated surface water carbonate system, nutrients, and relevant hydrochemical parameters in the inner Changjiang (Yangtze River) Estuary, covering its channel-like South Branch and the lagoon-like North Branch, shortly after a spring-tide period in April 2010. In the North Branch, with a water residence time of more than 2 months, biogeochemical additions of ammonium (7.4 to 65.7 µmol kg^{-1}) and alkalinity (196 to 695 µmol kg^{-1}) were detected along with high salinity of 4.5 to 17.4. In the South Branch upper-reach, unusual salinity values of 0.20 to 0.67 were detected, indicating spillover waters from the North Branch. The spillover waters enhanced the springtime Changjiang export fluxes of nutrients, dissolved inorganic carbon, and alkalinity. And they affected the biogeochemistry in the South Branch, by lowering water-to-air CO_2 flux and continuing the nitrification reaction. In the North Branch, pCO_2 was measured from 930 to 1518 µatm at the salinity range between 8 and 16, which was substantially higher than the South Branch pCO_2 of 700 to 1100 µatm. Based on field data analyses and simplified stoichiometric equations, we suggest that the North Branch CO_2 productions were quantified by biogeochemical processes combining organic matter decomposition, nitrification, $CaCO_3$ dissolution, and acid-base reactions in the estuarine mixing zone. Although our study is subject to limited temporal and spatial coverage of sampling, we have demonstrated a procedure to quantificationally constrain net CO_2 productions in eutrophic estuaries and/or coastal lagoons, by coupling the chemical dynamics of carbonate and dissolved inorganic nitrogen systems.

BGD
12, 6405–6443, 2015

1 Introduction

Large-river estuaries are important interfaces between continents and the oceans. They are biogeochemical hot spots since they receive large inputs of particulate matters, organic carbon, and nutrients from continents and oceans to support high rates of metabolism and/or chemical reactions. Significantly, CO_2 emission from estuaries, coastal lagoons, and salt marshes to the atmosphere has been proposed as an important component of the global carbon cycle (Frankignoulle et al., 1996, 1998; Cai and Wang, 1998). The global estuarine CO_2 emission rate has been estimated at 0.1 to 0.5 $Gt\,C\,yr^{-1}$ (Borges, 2005; Borges et al., 2005; Cai, 2011; Chen et al., 2013). Also the chemical dynamics in large-river estuaries and their biogenic element fluxes have global and/or regional impacts on marine biogeochemistry (e.g., Justić et al., 1995; Bricker et al., 2008; Liu et al., 2015).

So far, mechanisms supporting the estuarine CO_2 emission rates need to be better understood, especially in those eutrophic large-river estuaries. Cai (2011) suggested that respiration processes may not occur in the large-river estuaries due to short water transit or residence times. However, many medium to large rivers have forked estuaries. For example, the inner estuary of the Yangtze River (Changjiang) is divided into two primary branches by the Chong-ming Island (Fig. 1). The Channel-like South Branch is subject to very low respiration rates (Zhai et al., 2007), while the lagoon-like North Branch shows substantial additions of free CO_2 and dissolved organic matters (Zheng et al., 2011; Guo et al., 2014). We contend that, if the estuarine areas have a sufficient water residence time (such as the North Branch of the inner Changjiang Estuary), they may function as sites of terrestrial carbon incineration.

In addition, biogeochemistry of dissolved inorganic carbon and nutrients in the North Branch are rarely studied. How the North Branch biogeochemistry sustains the estuarine CO_2 additions reported by Zheng et al. (2011) remains unknown. Furthermore, the North Branch is occupied by saline water rather than freshwater, especially in relatively dryer seasons (He et al., 2006; Zheng et al., 2011; Guo et al., 2014). According

BGD
12, 6405–6443, 2015

to earlier results (e.g., Mao et al., 2001), the saltwater spillover from the North Branch usually occurs during spring-tide periods (with tidal ranges of more than 2.5 m) in winter and spring, with water discharge rates of lower than 25 000 $m^3 s^{-1}$ (from the Datong Station, ~ 400 km upstream of the study area). The saltwater spillover from the North Branch has received increasing attention since the occurrence of salty water in the South Branch threatens an important water source of Shanghai, the Qingcaosha Reservior (e.g., Shen et al., 1980; Mao et al., 2001; He et al., 2006; Wu et al., 2006; Xue et al., 2009; Qiu and Zhu, 2013). However, the potential impacts of spillover signals from the North Branch (Fig. 1a) on the budgets of carbon and nitrogen in the South Branch are poorly understood.

To evaluate the impacts of the North Branch saltwater spillover on the South Branch biogeochemistry, we investigated carbonate system and nutrients in the inner Changjiang Estuary in April 2010, covering both of the two primary branches (Fig. 1), shortly after a spring tide period. Together with simultaneous dissolved oxygen (DO) and partial pressure of CO_2 (pCO_2) data, this dataset also provides an opportunity to quantificationally examine how coupled dynamics of nitrogen and carbon elements affect CO_2 degassing fluxes from this important large-river estuary to the atmosphere, which may help to understand CO_2 dynamics and the controlling processes in those eutrophic large-river estuaries and coastal lagoons of the world.

2 Materials and methods

2.1 Study area

Changjiang is the fourth largest river in the world by virtue of the water discharge of ~ 944×10^9 $m^3 yr^{-1}$ (Dai and Trenberth, 2002). It exports large amounts of nutrients, alkalinity and carbon to the adjacent East China Sea (ECS) continental shelf (e.g., Chen and Wang, 1999; Wang and Wang, 2006; Zhang et al., 2007), enhancing the coastal eutrophication and red tides there (e.g., Chen et al., 2003; Zhou et al., 2008).

BGD
12, 6405–6443, 2015

Changjiang is also one of the most important solid transporting rivers (Gaillardet et al., 1999), although its downstream solid content has declined from $\sim 600\,mg\,L^{-1}$ in the 1960s to $< 400\,mg\,L^{-1}$ in the 2000s (Li and Zhang, 2003; Lin et al., 2007). Since its upstream water flows through the Yun–Gui Plateau and the Sichuan Basin, where the basement rocks are abundant in carbonates (Chen et al., 2002), the suspended sediment in the Changjiang River is rich of calcite (Chen et al., 2001). Also the Changjiang water is characterized by high alkalinity (Chen et al., 2002; Wu et al., 2007; Zhai et al., 2007) as compared with many other major rivers in the world.

The inner Changjiang Estuary is a large tidal estuary, complicated by bathymetry, islands, and deep channels (Xue et al., 2009). Nearly all of the river flow is transported via its South Branch into the ECS (Shen, 2001; Qu, 2010). The North Branch of the inner Changjiang Estuary is relatively shallow (water depth $\sim 3\,m$) and open to navigation only at high tides in a day. At low tide periods, however, the North Branch is isolated from the Changjiang main stream.

In the outer Changjiang Estuary, a coastal current (i.e., Yellow Sea Coastal Current, YSCC for short) affects the hydrology and hydrochemistry during the northeast monsoon period from October to April in the following year (Fig. 1a; Chen, 2009). This current has higher dissolved inorganic carbon (DIC) and total alkalinity (TAlk) as compared with most of ECS surface waters (Zhai et al., 2014).

2.2 Survey design

During 2 to 7 April 2010, a sampling cruise was carried out in the inner Changjiang Estuary. Shortly before the cruise, the water discharge rates (from the Datong Station) increased from $17\,600\,m^3\,s^{-1}$ in 27 March to $20\,800\,m^3\,s^{-1}$ in 2 April (Fig. 2a). Therefore, this cruise represented a transitional period between the dry seasons (usually with the water discharge rate of less than $14\,000\,m^3\,s^{-1}$, from December of the last year to February) and the flood seasons (usually with the water discharge rate of more than $40\,000\,m^3\,s^{-1}$, from May to September). Overall, our cruise included three surveys/legs in the South Branch, one survey in the North Branch, and one survey in

BGD
12, 6405–6443, 2015

the outer Changjiang Estuary. The three South Branch surveys occupied the 3rd day, 6th day, and 7th day after the spring-tide day in 1 April (Fig. 2b). In the North Branch, two anchored stations were repeatedly sampled for 12 to 20 h against tide height and salinity variations.

2.3 Sampling and analyses

Using an underway pumping system similar to Zhai et al. (2005, 2007), surface water (at a depth of ~ 1 m) was pumped from a side intake for continuous measurements of hydrochemical parameters such as temperature, salinity, DO and pCO_2. Via a side vent of our pumping system, discrete samples for Winkler DO, pH, DIC, TAlk, nutrients and particulate matters were collected at selected sites (Fig. 1).

Surface water temperature and salinity were continuously determined with a pre-calibrated YSI® 6600 m, with the precisions of ±0.01 °C and ±0.01 salinity units. And the underway salinity data were validated by simultaneous discrete salinity data. Aqueous pCO_2 was continuously detected by a Li-Cor® non-dispersive infrared spectrometer (Li-7000) together with a continuous flow and fully sealed cylinder-type equilibrator (Zhai et al., 2007; Jiang et al., 2008). For calibration purposes, four CO_2 gas standards with CO_2 molecular fractions from 400 to 1510 µmol mol^{-1} were applied. The uncertainty of these standards was ~ 1 %, which represents the maximum level of uncertainty during the period of extensive measuring of pCO_2 and data processing (see details in Zhai et al., 2005). The field-measured atmospheric CO_2 data were corrected to survey-based barometric pressure at 10 m above the water surface and 100 % humidity at water surface temperature and salinity, following the procedure described in Zhai et al. (2007).

For discrete salinity measurements, water samples were sealed in 140 mL high-density polyethylene bottles and kept at room temperature. They were determined in a week using a WTW TetraCon® 325 probe based on conductivity measurements, with a precision of ±0.1 salinity units (Yan et al., 2012). Winkler DO and NIST (National In-

BGD
12, 6405–6443, 2015

stitute of Standards and Technology, USA)-traceable pH (at 15 °C) were sampled and determined according to Zhai et al. (2007, 2012). The possible nitrite interference in the DO titration was removed by adding 0.01 % NaN_3 during sample fixation (Wong, 2012). pH was measured on board using a precision pH meter and an Orion® 8102BN Ross electrode, which were calibrated against three NIST-traceable buffers (pH = 4.00, 7.03, and 10.12 at 15.0 °C, Thermo Fisher Scientific Inc., USA). The precisions of DO and pH data were ±0.5 % DO and ±0.01 pH, respectively (Zhai et al., 2012). To express the oxygen consumption during water mixing, DO saturation was calculated from field-measured DO concentrations divided by DO concentration at equilibrium with the atmosphere. The latter was calculated as per the Benson and Krause (1984) equation.

For measurements of nutrient elements and TAlk, trinary water samples were filtered on board with 0.45 µm cellulose acetate membranes (Zhai et al., 2007; Yan et al., 2012). One of these was poisoned with 0.1 % chloroform and preserved at 4 °C for NH_4^+–N (ammonium) and silicate determination (within a time frame of 10 days upon sampling). The second one was deep-frozen and kept at −20 °C for NO_3^-–N (nitrate), NO_2^-–N (nitrite) and phosphate determination (within a time frame of 25 days upon sampling). The third one (for TAlk) was stored in a 140 mL high-density polyethylene bottle, immediately mixed with 50 µL of saturated $HgCl_2$, and then sealed and preserved at room temperature until determination (within a time frame of 15 days upon sampling). Water samples for DIC were unfiltered but allowed to settle before measurement. They were stored in 60 mL borosilicate glass bottles (bubble free), and also preserved with 50 µL of saturated $HgCl_2$ and determined within a time frame of 7 days upon sampling.

Water samples for suspended particulate matter (SPM), particulate organic carbon (POC), and particulate inorganic carbon (PIC) were filtered on board with carbon-free 0.7 µm quartz microfiber (GFF) membranes. The SPM data were collected after drying in an oven at 50 °C. And then the membranes were divided into two equal parcels. One of them was prepared for total particulate carbon measurements (without acid fuming), and another one was fumed with concentrated HCl so as to remove carbonate before POC determination. Both total particulate carbon and POC were measured according

BGD
12, 6405–6443, 2015

to the JGOFS protocols (Knap et al., 1996), using a PE-2400 SERIES II CHNS/O analyzer. Finally, the PIC data were obtained from the difference between total particulate carbon and POC.

NO_3^-–N, NO_2^-–N, and phosphate were determined using an AA3 Auto-Analyzer (Bran + Luebbe Co., Germany), while NH_4^+–N and silicate were measured using a Tri-223 continuous Auto-Analyzer (see details in Yan et al., 2012). Briefly, NO_3^-–N and NO_2^-–N were measured by reducing NO_3^- to NO_2^- with a Cd column, and then determining NO_2^- using the standard pink azo dye spectrophotometric method. Phosphate, silicate and NH_4^+–N were measured based on the standard phospho-molybdenum blue, silicon molybdenum blue and indophenol blue spectrophotometric procedures. Note that an appropriate quantity of more reagent NaOH was added during the NH_4^+–N measurement so as to make the final pH within the optimum range of 10.5 ± 0.1 (Pai et al., 2001; Tzollas et al., 2010).

Following Zhai et al. (2007), DIC was measured by infrared detection after acid extraction of a 0.5 mL sample with a Kloehn® digital syringe pump, while TAlk was determined by Gran acidimetric titration on a 25 mL sample with another Kloehn® digital syringe pump, using a precision pH meter and an Orion® 8102BN Ross electrode for detection. To ensure the measuring quality of DIC and TAlk, certificated reference materials from Andrew G. Dickson's laboratory (Scripps Institute of Oceanography) were regularly checked at a precision of $\pm 2\,\mu mol\,kg^{-1}$.

2.4 Flux estimation

Riverine element export fluxes were estimated based on the element concentrations at the river end, i.e. west side of the Chongming Island (Fig. 1a). Water discharge data needed were measured at the Datong Station, as released by the China Bureau of Hydrology (http://xxfb.hydroinfo.gov.cn/). The North Branch saltwater spillover induced element fluxes were estimated based on a mass balance approach. See Sects. 4.1 and 4.4 for details.

BGD
12, 6405–6443, 2015

2.5 Calculating carbonate system parameters from DIC and TAlk

For the purpose of modeling calculations, aqueous pCO_2 and concentrations of bicarbonate and carbonate ions were calculated from the DIC, TAlk, silicate, phosphate, seawater temperature, and salinity values using the program CO2SYS.xls (Pelletier et al., 2011), an updated version of the original CO2SYS.EXE (Lewis and Wallace, 1998). The dissociation constants for carbonic acid were those determined by Millero et al. (2006), and the dissociation constant for the HSO_4^- ion was determined as per Dickson (1990).

3 Results

3.1 Hydrological and particle backgrounds

During the cruise, water temperature ranged from 10.6 to 13.8 °C. In the North Branch, water temperature was detected as low as 10.9 ± 0.3 °C, lower than the nearby offshore sea surface temperature observed in early spring (Zhai et al., 2014). The relatively high temperature of > 13 °C was only detected in the South Branch.

Salinity in the South Branch varied day by day (Fig. 3a). In the 3rd day after the spring-tide day, it ranged from 0.13 to 0.67, with a salinity peak at 121°22′ E (Fig. 3a), ~ 20 km downstream the west side of the Chong-ming Island. In the 6th day after the spring-tide day, it changed from 0.23 to 0.54, with a peak at ~ 40 km downstream the earlier salinity peak (Fig. 3a). These patterns were similar to results reported by He et al. (2006). In the 7th day after the spring-tide day, the salinity peak in the South Branch moved to downstream further, while salinity at the upstream and middle stations ranged from 0.14 to 0.16 (Fig. 3a). In the North Branch, however, very high salinity of 4.5 to 17.4 was determined in the surface water (Fig. 1b), showing the occupation of saline water (He et al., 2006; Zheng et al., 2011; Guo et al., 2014). East to the line of

BGD
12, 6405–6443, 2015

122° E, surface salinity ranged from 0.23 to 18.4, showing the combined influences of Changjiang dilution and YSCC waters (Fig. 1a; Zhai et al., 2014).

The South Branch SPM ranged from 25 to 202 mg L^{-1}. It was lower than earlier SPM values of 240 to 720 mg L^{-1} between 1960 and 2001 (Li and Zhang, 2003), but similar to recent SPM data of 20 to 190 mg L^{-1} between 2003 and 2005 (Lin et al., 2007). In the North Branch, however, surface water SPM was at very high levels of 390 to 455 mg L^{-1}, with POC of 259 to 417 µmol L^{-1} and PIC of 253 to 293 µmol L^{-1}. Particle related data are presented in the Appendix (Fig. A1) for public reference.

3.2 Distributions of hydrochemical parameters in the South Branch

In the South Branch, surface water DO saturation ranged from 86 to 93 % (Fig. 3b), similar to previous results reported by Zhai et al. (2007). In contrast, pH varied well and declined slightly from 3 April to 7 April (Fig. 3c). In 3rd day after the spring-tide day, pH showed a peak value of 8.06 at the site with the highest salinity. In 6th day after the spring-tide day, although the salinity varied from 0.23 to 0.54, pH ranged smoothly from 7.88 to 7.94. During the last survey in 7 April, pH ranged from 7.75 to 7.88.

NH_4^+–N ranged from 5.0 to 25.2 µmol kg^{-1} (Fig. 3d), while NO_2^-–N declined from 4.05–4.36 µmol kg^{-1} at our upstream stations to 2.03 µmol kg^{-1} at the river mouth stations (Fig. 3e). As the products from chemical fertilizer application and soil erosion in the drainage basin of Changjiang, riverine NO_3^-–N ranged from 126.5 to 139.9 µmol kg^{-1} (Fig. 3f). The concentration of NO_3^-–N was one or two magnitudes higher than those of NH_4^+–N and NO_2^-–N. To sum up, the concentration of dissolved inorganic nitrogen (DIN, the sum of concentrations of NH_4^+–N, NO_2^-–N, and NO_3^-–N) ranged from 142.2 to 167.3 µmol kg^{-1} (Fig. 3g). Except for a sampling site presumably influenced by a sewage outlet (Chai et al., 2006), the distributions of the two major DIN species (NH_4^+–N and NO_3^-–N) in the surface water roughly reflected the salinity variation patterns (Fig. 3). Considering the above-mentioned salty water mass, most NH_4^+–N data in 3 April were higher than those in 6 April (Fig. 3d), while most NO_3^-–N

BGD
12, 6405–6443, 2015

data showed an inverse trend (Fig. 3f). DIN in this water mass slightly declined during the three days from 3 April to 6 April (Fig. 3g).

As a particle-concentrated element (e.g., Das et al., 2006; Leote et al., 2013), phosphate was measured at relatively low levels from 0.87 to 1.63 $\mu mol\,kg^{-1}$ (Fig. 3h). However, silicate was at relatively high levels from 99.6 to 104.9 $\mu mol\,kg^{-1}$ (Fig. 3i).

Except for the sampling site presumably influenced by sewage, the two carbonate system parameters (i.e. TAlk and DIC) also reflected the salinity variation patterns (Fig. 3l and m). TAlk ranged from 1495 to 1694 $\mu mol\,kg^{-1}$, while DIC ranged from 1520 to 1654 $\mu mol\,kg^{-1}$.

The South Branch pCO_2 ranged from 628 to 1148 µatm (Fig. 3n). Its distribution patterns roughly mirrored the distributions of pH (Fig. 3). Similar to earlier results reported by Zhai et al. (2007) and Chen et al. (2008), pCO_2 was always higher than the water-air equilibration level of 398 to 411 µatm (Fig. 3n). Hydrochemical parameters against salinity in the South Branch are plotted in the Appendix (Fig. A2) for public reference.

3.3 Water mixing behaviors of hydrochemical parameters in the North Branch and the outer estuary area

In the North Branch, surface water DO saturation ranged from 83 to 95 % (Fig. 4a). Low DO saturation values of < 86 % were mostly observed at the middle salinity from 8.4 to 12.4. Correspondingly, significant additions of pCO_2 and NH_4^+–N were detected (Fig. 4). And the associated pH was measured at relatively low level from 7.90 to 7.92 (Fig. 4b). NO_2^-–N, NO_3^-–N and DIN also showed additions (Fig. 4e–g). However, silicate behaved like a conservative element (Fig. 4i), with a very tight linear relationship against salinity (n = 13, r = 0.9993).

In the outer estuary area, only two stations were sampled for nutrient analyses. Silicate data in both the outer area and the South Branch followed the water mixing line obtained from the North Branch (Fig. 4i), suggesting that water mixing in the outer area was controlled by nearly the same end-members as those in the North Branch. Therefore, we assumed conservative water mixing lines of dissolved nitrogen species in the

BGD
12, 6405–6443, 2015

Changjiang Estuary (Fig. 4). They were:

$$NH_4^+\text{–}N^{\text{conservative}}\ (\mu\text{mol kg}^{-1}) = -0.3041 \times \text{Salinity} + 12.5 \quad (1)$$

$$NO_2^-\text{–}N^{\text{conservative}}\ (\mu\text{mol kg}^{-1}) = -0.1163 \times \text{Salinity} + 2.5 \quad (2)$$

$$NO_3^-\text{–}N^{\text{conservative}}\ (\mu\text{mol kg}^{-1}) = -4.1905 \times \text{Salinity} + 135 \quad (3)$$

$$\text{DIN}^{\text{conservative}}\ (\mu\text{mol kg}^{-1}) = -4.6667 \times \text{Salinity} + 150 \quad (4)$$

where seawater end-members of NO_3^-–N ($\sim 3\,\mu\text{mol kg}^{-1}$ at a salinity of 31.5) and DIN ($\sim 10\,\mu\text{mol kg}^{-1}$ at a salinity of 30) referred to spring YSCC values reported by Chen et al. (2009) and Wang et al. (2003).

TAlk and DIC also showed additions in the North Branch, while they behaved like conservative elements in the outer area (Fig. 5). In the outer area, the simplified water mixing lines of TAlk and DIC, with seawater end-members of them from YSCC obtained in April 2007 (Zhai et al., 2014), were as follow:

$$\text{TAlk}^{\text{conservative}}\ (\mu\text{mol kg}^{-1}) = 22.068 \times \text{Salinity} + 1580 \quad (5)$$

$$\text{DIC}^{\text{conservative}}\ (\mu\text{mol kg}^{-1}) = 14.551 \times \text{Salinity} + 1600 \quad (6)$$

Most of field-measured TAlk and DIC values in the outer area satisfactorily followed Eqs. (5) and (6) (Fig. 5), giving confidence in the water mixing line reduction. The intercepts of Eqs. (5) and (6) were consistent with TAlk and DIC values at the river mouth (1595 to 1615 $\mu\text{mol kg}^{-1}$), and slightly higher than TAlk and DIC values at the river end (1495 to 1585 $\mu\text{mol kg}^{-1}$) (Fig. 3). However, they were $\sim 200\,\mu\text{mol kg}^{-1}$ lower than the freshwater end-member values of TAlk and DIC in spring of 2006 and 2007 ($\sim 1800\,\mu\text{mol kg}^{-1}$) (Zhai et al., 2007, 2014).

The assumed conservative mixing line of pCO_2 (Fig. 4c) was calculated from conservative TAlk (Eq. 5), DIC (Eq. 6), silicate (Fig. 4i), and a fixed phosphate of $1.4\,\mu\text{mol kg}^{-1}$ (Fig. 4h). It was a sunken line, with an oversaturated pCO_2 value of 596 µatm at salinity 1 and undersaturated pCO_2 value of 325 µatm at salinity 20. The freshwater end-member value was similar to field-measured pCO_2 at the river moth (Fig. 4c), while

BGD
12, 6405–6443, 2015

the relatively high-salinity value was consistent with the earlier reported YSCC pCO_2 range of 310 to 377 µatm obtained in April 2007 (Zhai et al., 2014).

To better evaluate the biogeochemical additions/removals of nitrogen and carbon elements, we calculated the conservative concentrations of DIN species and carbonate system parameters at salinity, according to Eqs. (1)–(6). And then we obtained the differences between the measured concentrations and the conservative concentrations along the mixing lines, i.e., ΔNH_4^+-N, ΔNO_2^--N, ΔNO_3^--N, ΔDIN, ΔTAlk and ΔDIC in Eqs. (7)–(12), with positive values indicating biogeochemical additions and negative values indicating removals. Note that both of the additions and removals are relative to the conservative mixing between the Changjiang freshwater end-member near the river mouth and the spring YSCC surface water end-member.

$$\Delta NH_4^+-N = [NH_4^+-N] - [NH_4^+-N^{\,conservative}] \quad (7)$$

$$\Delta NO_2^--N = [NO_2^--N] - [NO_2^--N^{\,conservative}] \quad (8)$$

$$\Delta NO_3^--N = [NO_3^--N] - [NO_3^--N^{\,conservative}] \quad (9)$$

$$\Delta DIN = \left([NH_4^+-N] + [NO_2^--N] + [NO_3^--N]\right) - DIN^{\,conservative} \quad (10)$$

$$\Delta TAlk = TAlk - TAlk^{\,conservative} \quad (11)$$

$$\Delta DIC = DIC - DIC^{\,conservative} \quad (12)$$

Figure 6 summarizes ΔNH_4^+-N, ΔNO_2^--N, ΔNO_3^--N, ΔDIN, ΔDIC and ΔTAlk against salinity in the North Branch. During our survey, biogeochemical additions of DIN species and carbonate system parameters were estimated at 7.4 to 65.7 µmol kg^{-1} (ΔNH_4^+-N), 1.24 to 16.15 µmol kg^{-1} (ΔNO_2^--N), 6.3 to 26.0 µmol kg^{-1} (ΔNO_3^--N), 27 to 103 µmol kg^{-1} (ΔDIN), 243 to 753 µmol kg^{-1} (ΔDIC), and 196 to 695 µmol kg^{-1} (ΔTAlk). Except for ΔNO_3^--N, most of those biogeochemical additions were obtained at salinity between 8 and 16 (Fig. 6), suggesting the associated biogeochemical processes mainly occurred at the middle salinity area.

BGD
12, 6405–6443, 2015

4 Discussion

4.1 Residence time estimation

Estuaries are not only transport passages of terrestrial materials from the continents to the oceans, but also chemical reactors and/or buffers (Officer, 1979). Before discussing biogeochemical processes and element transport fluxes in the inner Changjiang Estuary, the residence times need to be examined. To estimate the residence times, we balanced water and salt budgets under the condition of the North Branch saltwater spillover shortly after the spring-tide period:

$$Q_S = Q_R + Q_N \quad (13)$$

$$Q_S \times S_S = Q_R \times S_R + Q_N \times S_N \quad (14)$$

where Q_S, Q_R and Q_N are water discharges from the South Branch, from the upper river, and the mean water flux of the North Branch saltwater spillover during the spring-tide period in early April 2010 (Fig. 1a); S_S, S_R and S_N are mean salinity of the South Branch water, the Changjiang River water and the North Branch water. In this study, Q_R and S_R were 20 000 $m^3 s^{-1}$ and 0.14, respectively (Figs. 2a and 3a). S_S and S_N were estimated at 0.30 and 15.26, based on a compilation of our underway data obtained from 2 to 5 April (data partially reported in Figs. 1b and 3a). Therefore, Q_S and Q_N were estimated at 20 214 and 214 $m^3 s^{-1}$, respectively (Table 1).

Based on Shen (2001), Meng and Cheng (2005), the navigation map (2010 edition), and our field records, mean water depths of the South Branch (d_S) and the North Branch (d_N) were estimated at 8 and 3 m, respectively, while water areas of the South Branch (A_S) and the North Branch (A_N) were 900 and 422 km^2, respectively (Table 1). Therefore, the mean residence times of the North Branch water (τ_N) and the South

BGD
12, 6405–6443, 2015

Branch water (τ_S) were estimated as bellow:

$$\tau_N = A_N \times d_N/Q_N = 5.9 \times 10^6\,\mathrm{s} = 68\,\mathrm{day} \quad (15)$$

$$\tau_S = A_S \times d_S/Q_S = 0.36 \times 10^6\,\mathrm{s} = 4\,\mathrm{day} \quad (16)$$

We must point out that Eq. (16) ignored the tidal effect. That is, effluent water particles across the interface between inner and outer estuaries can return to the inner estuary (i.e., the South Branch) during the next tide cycle, leading to a longer exposure time of water particles than the steady-state residence time (Monsen et al., 2002). Based on Fig. 3a, the North Branch saltwater spillover (presumably in 1 April) induced salinity peak in the South Branch moved from 121°22′ E in 3 April to 121°50′ E in 6 April. Even in 7 April, the salinity peak was still observable inside the river mouth (west of 122°00′ E) (Fig. 3a). Thus the South Branch water was exposed to the estuarine biogeochemical processes for ∼ 7 days in spring, more than 1.5 times of the residence time estimated under the steady-state assumption via Eq. (16).

Similar to the South Branch, the exposure time of the North Branch water estimated via the steady-state Eq. (15) is also subject to uncertainties. However, Eq. (15) suggested that the North Branch water had a very long residence time of more than 2 months in spring. It provided reaction times for many biogeochemical processes to function.

4.2 Maintaining mechanisms of the biogeochemical additions in the North Branch

In the North Branch, DIC and TAlk were linearly correlated ($n = 13$, $r = 0.996$), with a slope of 0.9888 that was very close to 1 (Fig. 7a). Since DIC is the sum of free CO_2, HCO_3^- and CO_3^{2-}, and TAlk = $[HCO_3^-] + 2[CO_3^{2-}] + [B(OH)_4^-] + [OH^-] - [H^+]$ + other trace species, Fig. 7a suggested that both DIC and TAlk in the North Branch were mainly composed of HCO_3^- ion. Note that this pattern was much different from the usual DIC vs. TAlk plot (with a slope lower than 0.5) as driven by water mixing between the Changjiang freshwater and ECS seawaters (Zhai et al., 2007).

BGD
12, 6405–6443, 2015

ΔTAlk and ΔDIN were also linearly correlated in the North Branch (n = 13, r = 0.985), with a slope of 6.56 (Fig. 7b). This plot suggested that both the carbonate system and dissolved inorganic nitrogen dynamics in the North Branch might controlled by same biogeochemical processes. To examine these processes from a quantitative point of view, we analyzed the stoichiometric relationship of the Redfield respiration. Also resolved were the nitrification, the $CaCO_3$ dissolution, and the acid–base reaction during the oxidation of organic matters.

In a saline aquatic environment with abundant oxygen and the pH of ~ 8, the Redfield respiration of biogenic organic matters is directly associated with a release of NH_4^+–N:

$$(CH_2O)_{106}(NH_3)_{16}H_3PO_4 + 106O_2 \rightarrow 92CO_2 + 16NH_4^+ + 14HCO_3^- + HPO_4^{2-} + 92H_2O \quad \text{(R1)}$$

As compared with the decomposition of organic matters, the oxidation of NH_4^+–N (a key step of nitrification) is a time-expensive reaction (e.g., Dai et al., 2008), especially when the temperature is lower than 15 °C. The nitrification occurs as below:

$$2NH_4^+ + 3O_2 + 4HCO_3^- \rightarrow 2NO_2^- + 4CO_2 + 6H_2O \quad \text{(R2)}$$

$$2NO_2^- + O_2 \rightarrow 2NO_3^- \quad \text{(R3)}$$

Combining Reactions (R1)–(R3), a complete Redfield respiration of biogenic organic matters is:

$$(CH_2O)_{106}(NH_3)_{16}H_3PO_4 + 138O_2 + 18HCO_3^- \rightarrow 124CO_2 + 16NO_3^- + HPO_4^{2-} + 140H_2O \quad \text{(R4)}$$

In the North Branch, these processes were associated with the consumption of DO and the releases of free CO_2 and the three dissolved inorganic nitrogen species (Fig. 4). To reveal how many NH_4^+–N released through respiration were transformed into NO_2^-–N and/or NO_3^-–N, we plotted ΔNH_4^+–N vs. ΔDIN (Fig. 7c). The North Branch ΔNH_4^+–N and ΔDIN were linearly correlated (n = 13, r = 0.94), with a slope of 0.63. This slope

BGD
12, 6405–6443, 2015

suggested that Reactions (R2) and (R3) may only transform (1 – 0.63) × 100 % = 37 % of respiration-induced DIN additions into NO_2^-–N and/or NO_3^-–N. Combining Reactions (R1) and (R4) based on this ratio, ignoring the incomplete nitrite oxidation, the local status of Redfield respiration in the North Branch was better characterized as below:

$$(CH_2O)_{106}(NH_3)_{16}H_3PO_4 + 118O_2 \rightarrow$$
$$104CO_2 + 10NH_4^+ + 6NO_3^- + 2HCO_3^- + HPO_4^{2-} + 110H_2O \quad \text{(R5)}$$

Furthermore, the North Branch was an environment with abundant supplies of PIC (mostly calcite or $CaCO_3$) and seawater (having the CO_3^{2-} ion). Besides CO_2 degassing, most of the above-mentioned estuarine CO_2 productions are potentially removed by $CaCO_3$ dissolution (Abril et al., 2003) and/or CO_3^{2-} titration:

$$CO_2 + CaCO_3 + H_2O \rightarrow Ca^{2+} + 2HCO_3^- \quad \text{(R6)}$$

$$CO_2 + CO_3^{2-} + H_2O \rightarrow 2HCO_3^- \quad \text{(R7)}$$

Except for the CO_3^{2-} titration (Reaction R7), all of respiration (Reaction R5), nitrification (Reaction R2) and $CaCO_3$ dissolution (Reaction R6) affected the ratio of ΔDIC to ΔTAlk (Fig. 7d). In the North Branch, both ΔDIC and ΔTAlk were positive, suggesting net biogeochemical additions. ΔDIC = 1.09 × ΔTAlk (n = 13, r = 0.992). The slope of 1.09 (higher than the $CaCO_3$ dissolution induced slope of 0.5) suggested that respiration and $CaCO_3$ dissolution controlled the North Branch carbonate system as below:

$$(CH_2O)_{106}(NH_3)_{16}H_3PO_4 + 118O_2 + 88CaCO_{3(s)} \rightarrow$$
$$16CO_2 + 88Ca^{2+} + 178HCO_3^- + 10NH_4^+ + 6NO_3^- + HPO_4^{2-} + 22H_2O \quad \text{(R8)}$$

In the South Branch, however, most ΔDIC and ΔTAlk were negative, suggesting biogeochemical removals. ΔDIC = 0.66 × ΔTAlk – 21 μmol kg^{-1} (Fig. 7d). The slope of 0.66 together with the negative ΔDIC and ΔTAlk values suggested that both CO_2 degassing

BGD
12, 6405–6443, 2015

and nitrification controlled the South Branch carbonate system (Fig. 7d). The later process was also evidenced by the above-mentioned dissolved nitrogen system dynamics in Fig. 3. Although $CaCO_3$ dissolution may also occur in the South Branch, as indicated by the facts that several ΔDIC and ΔTAlk plots in the South Branch were positive, and the slope of 0.66 was similar to the $CaCO_3$ dissolution induced slope of 0.5 (Fig. 7c), its effects on the South Branch carbonate system were negligible (Zhai et al., 2007).

In summary, the biogeochemical additions of NH_4^+–N and carbonate observed in the North Branch were driven by the biogeochemical processes combining organic matter decomposition, nitrification, and $CaCO_3$ dissolution, as described by Reaction (R8). Abundant organic matters and $CaCO_3$ particles, together with the quite long residence time and suitable environmental conditions such as temperature and oxygen, had made the North Branch into a natural reactor. This big reactor affected both element export fluxes (via its water spillover, see Sect. 4.4) and the water-to-air CO_2 flux in this important estuary (via increasing aqueous pCO_2, see Sect. 4.3).

4.3 Estuarine CO_2 dynamics in the North Branch

Reaction (R8) suggested that, if most of estuarine CO_2 products from Redfield respirations are removed by $CaCO_3$ dissolution, the ratio of ΔTAlk to ΔDIN should be 176/16 = 11.125. Alternatively, if none of the CO_2 products is removed by the $CaCO_3$ dissolution, the ratio of ΔTAlk to ΔDIN should be 2/16 = 0.125 based on Reaction (R5). Therefore, the real ratio of ΔTAlk to ΔDIN of 6.56 (Fig. 7b) suggested that only 6.56/(11.125 – 0.125) × 100 % = 60 % of respiration-induced free CO_2 was removed via $CaCO_3$ dissolution. Ignoring the minor impacts of CO_2 degassing fluxes (due to the much slower air-water exchanging rates as compared with the acid–base reactions), the other 40 % of estuarine CO_2 products were potentially titrated by CO_3^{2-} ion supplied by the seawater end-member, as indicated by Reaction (R7).

To discuss this effect, we calculated $pCO_2^{addition}$ in the North Branch via pCO_2 minus $pCO_2{}^{conservative}$, based on Fig. 4c. We then calculated concentrations of the additional

BGD
12, 6405–6443, 2015

free CO_2, using $[CO_2^*]^{addition} = K_H \times pCO_2^{addition}$, where K_H is the solubility coefficient of CO_2, calculated via the Weiss (1974) equation. Figure 8a showed that $[CO_2^*]^{addition}$ ranged from 2.7 to 53 µmol kg^{-1} in the North Branch, usually lower than those predicted values based on Reaction (R8) and our ΔDIN data. The differences were likely caused by acid-base titration between respiration-induced free CO_2 and seawater-introduced CO_3^{2-} ion.

Figure 8b showed that conservative concentrations of non-carbonate alkalinity (such as borate ions) ranged from 7 µmol kg^{-1} at salinity 4 to 30 µmol kg^{-1} at salinity 16. These non-carbonate alkalinity values primarily accounted for the observed differences between TAlk and DIC in the North Branch, i.e. 22 to 29 µmol kg^{-1} as suggested by Fig. 7a. This comparison provided another evidence supporting the idea that seawater-introduced $[CO_3^{2-}]^{conservative}$ was mostly titrated by respiration-induced CO_2, and transferred into HCO_3^- ions.

Furthermore, we regarded the conservative concentrations of CO_3^{2-} ion (Fig. 8b) as the maximum removals via CO_3^{2-} titration. Figure 8a showed that the predicted values via DIN minus $[CO_3^{2-}]^{conservative}$ were highly consistent with the field-measured values of $[CO_2^*]^{addition}$ at salinity of 5 to 13, indicating that seawater-introduced $[CO_3^{2-}]^{conservative}$ was fully titrated by respiration-induced CO_2. However, the predicted values were lower than the real at salinity of > 13, presumably due to the overestimate of CO_3^{2-} titration reactions there.

In summary, we have quantificationally demonstrated that the observed aqueous pCO_2 in the North Branch was determined by water mixing and several biogeochemical processes. Although 80 to 85 % of estuarine CO_2 production from organic matter decomposition and nitrification had been removed by $CaCO_3$ dissolution (~ 60 %) and CO_3^{2-} titration (50 to 60 % of the residuals, Fig. 8), the North Branch acted as a significant source area of the atmospheric CO_2 with higher pCO_2 than the South Branch (Fig. 4c). To determine the seasonality and magnitude of the North Branch water-to-air CO_2 flux, more investigations are needed.

BGD
12, 6405–6443, 2015

4.4 Spillover fluxes of TAlk, DIC, and nutrients from the North Branch into the Changjiang mainstream

The North Branch biogeochemical signals intrude to Changjiang mainstream (the South Branch) via the tide induced saltwater spillover process in dry seasons (Fig. 1a), potentially increasing element export fluxes to the ECS. Considering the steady state spillover flux of saline water ($\sim 214\,m^3\,s^{-1}$, Table 1) from the North Branch into the Changjiang mainstream, the spillover flux of salt was estimated at $3265\,kg\,s^{-1}$, slightly higher than the riverine transport salt flux (Table 2). Similar to the salt flux estimation, riverine transport fluxes and spillover fluxes of TAlk, DIC, and nutrients were calculated (Table 2).

Generally, spillover fluxes of TAlk, DIC, and nutrients from the North Branch into the Changjiang mainstream were minor, as compared with the Changjiang transport fluxes. However, the springtime areal yield rates of TAlk, DIC, and DIN species from the North Branch were 34 to 133 times higher than those from the Changjiang drainage basin, as Changjiang has a drainage area of 1.8×10^6 km^2 (Chen et al., 2002), roughly 4000 times of the North Branch water area. Note that the organic matters and $CaCO_3$ particles supporting the springtime TAlk, DIC, and DIN production in the North Branch were also supplied by Changjiang during its flood seasons. Therefore, the North Branch may serve as an estuarine chemical buffer, to some extent smoothing seasonal variations of Changjiang element export fluxes.

During our sampling period, the spillover of TAlk, DIC, and DIN species from the North Branch affected the biogeochemistry in the South Branch. Firstly, the spillover water transported more TAlk than DIC into the South Branch (Table 2), leading to the South Branch pCO_2 decline from ~ 1000 µatm at salinity of ~ 0.14 (with the water-to-air pCO_2 difference of ~ 600 µatm) to ~ 700 µatm at salinity of > 0.4 (with the water-to-air pCO_2 difference of ~ 300 µatm) (Fig. 3n). If the air-water gas transfer velocity was changeless, the 50 % decline of water-to-air pCO_2 difference means that the water-to-air CO_2 degassing flux had decreased by 50 % due to the spillover of salty water.

BGD
12, 6405–6443, 2015

Secondly, the spillover water likely contained active nitrifiers, which continued the nitrification reaction in the South Branch, as indicated by the NH_4^+–N decline and the NO_3^-–N increase of the salty water mass from 3 to 6 April (Fig. 3). This was also evidenced by the pH decline and the pCO_2 increase signals (at salinity of > 0.4) during the same period (Fig. 3), as shown by Reaction (R2).

5 Concluding remarks

This study showed that the spillover waters from the North Branch had minor contributions to the Changjiang transport fluxes of nutrients, dissolved inorganic carbon, and alkalinity. They affected the biogeochemistry in the South Branch, by lowering water-to-air CO_2 fluxes and continuing the nitrification. Significantly, several primary biogeochemical processes such as organic matter decomposition, nitrification, $CaCO_3$ dissolution, and acid-base reaction occurred in the North Branch of the Changjiang Estuary, leading to the unusual high pCO_2 values at middle salinity and the biogeochemical additions of dissolved inorganic nitrogen species and carbonate system parameters. Similar biogeochemical processes may occur in many eutrophic estuaries and/or coastal lagoons of the world. This study demonstrated a procedure to quantificationally analyze the coupled dynamics of dissolved inorganic nitrogen and carbonate systems, which may help to better understand the combined effects of metabolic processes and chemical reactions on CO_2 fluxes in estuaries and/or coastal lagoons with similar physical and biogeochemical conditions.

Appendix A: Distributions of surface particulate parameters

Particulate samples were collected at selected sites during our April 2010 cruise. Their suspended particulate matter concentrations, particulate organic carbon data, and particulate inorganic carbon data were presented against longitude (Fig. A1). Usually the North Branch had more SPM, POC, and PIC concentrations than the South Branch.

BGD
12, 6405–6443, 2015

Appendix B: Hydrochemical parameters vs. salinity in the south Branch

Despite the very low salinity, we plotted those ammonium, nitrate, dissolved inorganic nitrogen, partial pressure of CO_2, total alkalinity, and dissolved inorganic carbon data obtained in the South Branch against salinity (Fig. A2). From 3 to 6 April, we obtained a decline of ammonium and increases of nitrate and partial pressure of CO_2 in the same salinity range from 0.4 to 0.6, indicating nitrification.

Acknowledgements. We thank Di Qi for his assistance in collecting field data of pH, SPM, POC, and PIC. Yu-zhong Huang, Wei Tian, Wei Ma, Li-bin Zhou, and Yu Mo provided much help during the sampling survey. The research was jointly supported by the Oceanic Public Science and Technology Research Funds Projects under contract No. 201505003, and the National Natural Science Foundation of China through grant 41276061, and the Key Laboratory of Marine Ecosystem and Biogeochemistry of State Oceanic Administration, China (through open fund No. LMEB200802). Sampling survey was supported by the State Key Laboratory of Satellite Ocean Environment Dynamics, Second Institute of Oceanography of State Oceanic Administration, China (through open fund No. SOED0906). The dataset will be available as supplement if the manuscript is accepted for publication in Biogeosciences.

References

Abril, G., Etcheber, H., Delille, B., Frankignoulle, M., and Borges, A. V.: Carbonate dissolution in the turbid and eutrophic Loire estuary, Mar. Ecol.-Prog. Ser., 259, 129–138, doi:10.3354/meps259129, 2003.

Benson, B. B. and Krause, D.: The concentration and isotopic fractionation of oxygen dissolved in fresh water and seawater in equilibrium with the atmosphere, Limnol. Oceanogr., 29, 620–632, 1984.

Borges, A. V.: Do we have enough pieces of the jigsaw to integrate CO_2 fluxes in the coastal ocean?, Estuaries, 28, 3–27, doi:10.1007/BF02732750, 2005.

Borges, A. V., Delille, B., and Frankignoulle, M.: Budgeting sinks and sources of CO_2 in the coastal ocean: diversity of ecosystems counts, Geophys. Res. Lett., 32, L14601, doi:10.1029/2005GL023053, 2005.

BGD
12, 6405–6443, 2015

Bricker, S. B., Longstaff, B., Dennison, W., Jones, A., Boicourt, K., Wicks, C., and Woerner, J.: Effects of nutrient enrichment in the nation's estuaries: a decade of change, Harmful Algae, 8, 21–32, doi:10.1016/j.hal.2008.08.028, 2008.

Cai, W.-J.: Estuarine and coastal ocean carbon paradox: CO_2 sinks or sites of terrestrial carbon incineration?, Annu. Rev. Mar. Sci., 3, 123–145, doi:10.1146/annurev-marine-120709-142723, 2011.

Cai, W.-J. and Wang, Y.-C.: The chemistry, fluxes and sources of carbon dioxide in the estuarine waters of the Satilla and Altamaha Rivers, Georgia, Limnol. Oceanogr., 43, 657–668, 1998.

Chai, C., Yu, Z.-M., Song, X.-X., and Cao, X.-H.: The status and characteristics of eutrophication in the Yangtze River (Changjiang) Estuary and the adjacent East China Sea, China, Hydrobiologia, 563, 313–328, doi:10.1007/s10750-006-0021-7, 2006.

Chen, C.-S., Zhu, J.-R., Beardsley, R. C., and Franks, P. J. S.: Physical-biological sources for dense algal blooms near the Changjiang River, Geophys. Res. Lett., 30, 1515, doi:10.1029/2002GL016391, 2003.

Chen, C.-T. A.: Chemical and physical fronts in the Bohai, Yellow and East China seas, J. Marine Syst., 78, 394–410, doi:10.1016/j.jmarsys.2008.11.016, 2009.

Chen, C.-T. A. and Wang, S.-L.: Carbon, alkalinity and nutrient budget on the East China Sea continental shelf, J. Geophys. Res., 104, 20675–20686, 1999.

Chen, C.-T. A., Zhai, W.-D., and Dai, M.-H.: Riverine input and air–sea CO_2 exchanges near the Changjiang (Yangtze River) Estuary: status quo and implication on possible future changes in metabolic status, Cont. Shelf Res., 28, 1476–1482, doi:10.1016/j.csr.2007.10.013, 2008.

Chen, C.-T. A., Huang, T.-H., Chen, Y.-C., Bai, Y., He, X., and Kang, Y.: Air–sea exchanges of CO_2 in the world's coastal seas, Biogeosciences, 10, 6509–6544, doi:10.5194/bg-10-6509-2013, 2013.

Chen, J.-S., Wang, F.-Y., Xia, J.-H., and Zhang, L.-T.: Major element chemistry of the Changjiang (Yangtze River), Chem. Geol., 187, 231–255, 2002.

Chen, Q.-M., Qiu, Y.-Q., Chen, B.-L., and Chen, J.-Y.: The phase analysis of the suspended sediments and depositions in Changjiang Estuary by the X-ray Powder Diffraction method, J. East China Normal Univ. (Nat. Sci.), (1), 77–83, 2001 (in Chinese).

Dai, A.-G. and Trenberth, K. E.: Estimates of freshwater discharge from continents: latitudinal and seasonal variations, J. Hydrometeorol., 3, 666–687, 2002.

BGD
12, 6405–6443, 2015

Dai, M., Wang, L., Guo, X., Zhai, W., Li, Q., He, B., and Kao, S.-J.: Nitrification and inorganic nitrogen distribution in a large perturbed river/estuarine system: the Pearl River Estuary, China, Biogeosciences, 5, 1227–1244, doi:10.5194/bg-5-1227-2008, 2008.

Das, J., Patra, B. S., Baliarsingh, N., and Parida, K. M.: Adsorption of phosphate by layered double hydroxides in aqueous solutions, Appl. Clay Sci., 32, 252–260, doi:10.1016/j.clay.2006.02.005, 2006.

Dickson, A. G.: Standard potential of the reaction: $AgCl(s)+1/2H_2(g) = Ag(s)+HCl(aq)$, and the standard acidity constant of the ion HSO_4^- in synthetic sea water from 273.15 to 318.15 K, J. Chem. Thermodyn., 22, 113–127, 1990.

Frankignoulle, M., Bourge, I., and Wollast, R.: Atmospheric CO_2 fluxes in a highly polluted estuary (the Scheldt), Limnol. Oceanogr., 41, 365–369, 1996.

Frankignoulle, M., Abril, G., Borges, A., Bourge, I., Canon, C., Delille, B., Libert, E., and Théate, J.-M.: Carbon dioxide emission from European estuaries, Science, 282, 434–436, 1998.

Gaillardet, J., Dupré, B., Louvat, P., and Allègre, C. J.: Global silicate weathering and CO_2 consumption rates deduced from the chemistry of large rivers, Chem. Geol., 159, 3–30, 1999.

Guo, W.-D., Yang, L.-Y., Zhai, W.-D., Chen, W.-Z., Osburn, C. L., Huang, X., and Li, Y.: Runoff-mediated seasonal oscillation in the dynamics of dissolved organic matter in different branches of a large bifurcated estuary – the Changjiang Estuary, J. Geophys. Res.-Biogeo., 119, 776–793, doi:10.1002/2013JG002540, 2014.

He, S.-L., Ding, P.-X., and Kong, Y.-Z.: Dry-season salinity variations in the South Branch of the Changjiang Estuary and the saltwater intrusion from the North Branch, Prog. Nat. Sci., 16, 584–589, 2006 (in Chinese).

Jiang, L.-Q., Cai, W.-J., Wanninkhof, R., Wang, Y.-C., and Lüger, H.: Air–sea CO_2 fluxes on the U.S. South Atlantic Bight: spatial and seasonal variability, J. Geophys. Res., 113, C07019, doi:10.1029/2007JC004366, 2008.

Justić, D., Rabalais, N. N., and Turner, R. E.: Stoichiometric nutrient balance and origin of coastal eutrophication, Mar. Pollut. Bull., 30, 41–46, 1995.

Knap, A., Michaels, A., Close, A., Ducklow, H., and Dickson, A.: Protocols for the Joint Global Ocean Flux Study (JGOFS) core measurements, JGOFS Report No.19, available at: http://ijgofs.whoi.edu/Publications/Report_Series/reports.html (last access: 25 September 2010), 1996.

BGD
12, 6405–6443, 2015

Leote, C., Epping, E., and Cappellen, P. V.: Phosphate sorption from seawater solutions: particle concentration effect, Mar. Chem., 148, 52–62, doi:10.1016/j.marchem.2012.12.002, 2013.

Lewis, E. and Wallace, D. W. R.: Program developed for CO_2 system calculations, ORNL/CDIAC-105, Carbon Dioxide Information Analysis Center, Oak Ridge National Laboratory, US Department of Energy, Oak Ridge, Tennessee, 1998.

Li, J.-Y. and Zhang, J.: Variations of solid content and water chemistry at Nantong station and weathering processes of the Changjiang watershed, Resour. Environ. Yangtze Basin, 12, 363–369, 2003 (in Chinese).

Li, X.-A., Yu, Z.-M., Song, X.-X., Cao, X.-H., and Yuan, Y.-Q.: Nitrogen and phosphorus budgets of the Changjiang River estuary, Chin. J. Oceanol. Limn., 29, 762–774, doi:10.1007/s00343-011-0505-9, 2011.

Lin, J., Wu, Y., Zhang, J., Yang, S.-L., and Zhu, Z.-Y.: Seasonal variation of organic carbon fluxes in the Yangtze River and influence of Three-Gorges engineering, China Environ. Sci., 27, 246–249, 2007 (in Chinese).

Liu, K.-K., Yan, W.-J., Lee, H-J., Chao, S.-Y., Gong, G.-C., and Yeh, T.-Y.: Impacts of increasing dissolved inorganic nitrogen discharged from Changjiang on primary production and seafloor oxygen demand in the East China Sea from 1970 to 2002, J. Mar. Syst., 141, 200–217, doi:10.1016/j.jmarsys.2014.07.022, 2015.

Mao, Z.-C., Shen, H.-T., and Xiao, C.-Y.: Saltwater intrusion partterns in the Qingcaosha Area Changjiang River Estuary, Oceanol. Limnol. Sin., 32, 58–66, 2001 (in Chinese).

Meng, Y. and Cheng, J.: The atrophy of the estuarine North Branch of the Yangtze River, Mar. Geol. Lett., 21, 1–10, 2005 (in Chinese).

Millero, F. J., Graham, T. B., Huang, F., Bustos-Serrano, H., and Pierrot, D.: Dissociation constants of carbonic acid in seawater as a function of salinity and temperature, Mar. Chem., 100, 80–94, doi:10.1016/j.marchem.2005.12.001, 2006.

Monsen, N. E., Cloern, J. E., Lucas, L. V., and Monismith, S. G.: A comment on the use of flushing time, residence time, and age as transport time scales, Limnol. Oceanogr., 47, 1545–1553, 2002.

Officer, C. B.: Discussion of the behaviour of nonconservative dissolved constituents in estuaries, Estuar. Coast. Mar. Sci., 9, 91–94, 1979.

BGD
12, 6405–6443, 2015

Pai, S.-C., Tsau, Y.-J., and Yang, T.-I.: pH and buffering capacity problems involved in the determination of ammonia in saline water using the indophenol blue spectrophotometric method, Anal. Chim. Acta, 434, 209–216, 2001.
Pelletier, G. J., Lewis, E., and Wallace, D. W. R.: CO2SYS.XLS: a calculator for the CO_2 system in seawater for Microsoft Excel/VBA, Version 16, Washington State Department of Ecology, Olympia, Washington, 2011.
Qiu, C. and Zhu, J.-R.: Influence of seasonal runoff regulation by the Three Gorges Reservoir on saltwater intrusion in the Changjiang River Estuary, Cont. Shelf Res., 71, 16–26, doi:10.1016/j.csr.2013.09.024, 2013.
Qu, X.-F.: Hydrological characteristics of the North Branch, inner Changjiang Estuary: based on a field survey in August 2005, Chin. J. Water Resour. Res., 31(1), 30–33, 2010 (in Chinese).
Shen, H.-T.: Material Fluxes in the Changjiang Estuary, Beijing, China Ocean Press, 176 pp., 2001 (in Chinese).
Shen, H.-T., Mao, Z.-C., Gu, G.-C., and Xu, P.-L.: A preliminary study on the saltwater intrusion in the Changjiang Estuary, Yangtze River, (3), 20–26, 1980 (in Chinese).
Tzollas, N. M., Zachariadis, G. A., Anthemidis, A. N., and Stratis, J. A.: A new approach to indophenol blue method for determination of ammonium in geothermal waters with high mineral content, Int. J. Environ. An. Ch., 90, 115–126, doi:10.1080/03067310902962528, 2010.
Wang, B.-D. and Wang, X.-L.: Impact of the exceptionally high flood from the Changjiang River on the aquatic chemical distributions on the Huanghai Sea and East China Sea shelves in the summer of 1998, Acta Oceanol. Sin., 25, 43–52, 2006.
Wang, B.-D., Wang, X.-L., and Zhan, R.: Nutrient conditions in the Yellow Sea and the East China Sea, Estuar. Coast. Shelf S., 58, 127–136, 2003.
Wong, G. T. F.: Removal of nitrite interference in the Winkler determination of dissolved oxygen in seawater, Mar. Chem., 130/131, 28–32, doi:10.1016/j.marchem.2011.11.003, 2012.
Wu, H., Zhu, J.-R., Chen, B.-R., and Chen, Y.-Z.: Quantitative relationship of runoff and tide to saltwater spilling over from the North Branch in the Changjiang Estuary: a numerical study, Estuar. Coast. Shelf S., 69, 125–132, doi:10.1016/j.ecss.2006.04.009, 2006.
Wu, Y., Zhang, J., Liu, S.-M., Zhang, Z.-F., Yao, Q.-Z., Hong, G.-H., and Cooper, L.: Sources and distribution of carbon within the Yangtze River system, Estuar. Coast. Shelf S., 71, 13–25, doi:10.1016/j.ecss.2006.08.016, 2007.

BGD
12, 6405–6443, 2015

Xue, P.-F., Chen, C.-S., Ding, P.-X., Beardsley, R. C., Lin, H.-C., Ge, J.-Z., and Kong, Y.-Z.: Saltwater intrusion into the Changjiang River: a model-guided mechanism study, J. Geophys. Res., 114, C02006, doi:10.1029/2008JC004831, 2009.

Yan, X.-L., Zhai, W.-D., Hong, H.-S., Li, Y., Guo, W.-D., and Huang, X.: Distribution, fluxes and decadal changes of nutrients in the Jiulong River Estuary, Southwest Taiwan Strait, Chinese Sci. Bull., 57, 2307–2318, doi:10.1007/s11434-012-5084-4, 2012.

Zhai, W.-D., Dai, M.-H., Cai, W.-J., Wang, Y.-C., and Wang, Z.-H.: High partial pressure of CO_2 and its maintaining mechanism in a subtropical estuary: the Pearl River estuary, China, Mar. Chem., 93, 21–32, doi:10.1016/j.marchem.2004.07.003, 2005.

Zhai, W.-D., Dai, M.-H., and Guo, X.-H.: Carbonate system and CO_2 degassing fluxes in the inner estuary of Changjiang (Yangtze) River, China, Mar. Chem., 107, 342–356, doi:10.1016/j.marchem.2007.02.011, 2007.

Zhai, W.-D., Zhao, H.-D., Zheng, N., and Xu, Y.: Coastal acidification in summer bottom oxygen-depleted waters in northwestern–northern Bohai Sea from June to August in 2011, Chinese Sci. Bull., 57, 1062–1068, doi:10.1007/s11434-011-4949-2, 2012.

Zhai, W.-D., Chen, J.-F., Jin, H.-Y., Li, H.-L., Liu, J.-W., He, X.-Q., and Bai, Y.: Spring carbonate chemistry dynamics of surface waters in the northern East China Sea: water mixing, biological uptake of CO_2, and chemical buffering capacity, J. Geophys. Res.-Oceans, 119, 5638–5653, doi:10.1002/2014JC009856, 2014.

Zhang, J., Liu, S.-M., Ren, J.-L., Wu, Y., and Zhang, G.-L.: Nutrient gradients from the eutrophic Changjiang (Yangtze River) Estuary to the oligotrophic Kuroshio waters and re-evaluation of budgets for the East China Sea Shelf, Prog. Oceanogr., 74, 449–478, doi:10.1016/j.pocean.2007.04.019, 2007.

Zheng, M.-H., Zhang, H.-S., Pan, J.-M., Yu, P.-S., Liu, X.-Y., Zhang, H.-N., and Liu, J.-F.: Variations of seawater pCO_2 in the surface layer of the North Branch of Changjiang River Estuary in autumn, J. Mar. Sci., 29, 57–62, 2011 (in Chinese).

Zhou, M.-J., Shen, Z.-L., and Yu, R.-C.: Responses of a coastal phytoplankton community to increased nutrient input from the Changjiang (Yangtze) River, Cont. Shelf Res., 28, 1483–1489, doi:10.1016/j.csr.2007.02.009, 2008.

BGD
12, 6405–6443, 2015

Table 1. Summary of hydrological characteristics in the inner Changjiang Estuary during the spring-tide period in early Apr 2010. See the text for details.

	Water discharge ($m^3 s^{-1}$)	Salinity	Area (km^2)	Depth (m)
Upper river	$Q_R = 20\,000$	$S_R = 0.14$	–	–
South Branch	$Q_S = 20\,214$	$S_S = 0.30$	$A_S = 900$	$d_S = 8$
North Branch	$Q_N = 214$	$S_N = 15.26$	$A_N = 422$	$d_N = 3$

BGD
12, 6405–6443, 2015

Table 2. A steady-state estimation of Changjiang transport fluxes and the North Branch (NB) spillover fluxes of salt, TAlk, DIC, and nutrients during a spring-tide period in Apr 2010. See the text for details.

Chemical species	Changjiang transport	Spillover from the NB	% added by the NB
Water flux ($m^3\,s^{-1}$)	20 000[a]	214[a]	1.1 %
Salt flux ($kg\,s^{-1}$)	0.14[a] × 20 000 = 2800	15.26[a] × 214 = 3265	116 %
TAlk flux ($mol\,s^{-1}$)	1530[b] × 20 000/1000 = 30 600	(2336[c] × 214)/1000 = 500	1.6 %
DIC flux ($mol\,s^{-1}$)	1550[b] × 20 000/1000 = 31 000	(2310[c] × 214)/1000 = 494	1.6 %
NH_4^+–N flux ($mol\,s^{-1}$)	18[b] × 20 000/1000 = 360	(55[c] × 214)/1000 = 12	3.3 %
NO_2^-–N flux ($mol\,s^{-1}$)	4.2[b] × 20 000/1000 = 84	(11[c] × 214)/1000 = 2.4	2.9 %
NO_3^-–N flux ($mol\,s^{-1}$)	128[b] × 20 000/1000 = 2560	(102[c] × 214)/1000 = 22	0.9 %
DIN flux ($mol\,s^{-1}$)	150[b] × 20 000/1000 = 3000	(168[c] × 214)/1000 = 36	1.2 %
Phasphate flux ($mol\,s^{-1}$)	1.3[b] × 20 000/1000 = 26	(1.3[c] × 214)/1000 = 0.28	1.1 %
Silicate flux ($mol\,s^{-1}$)	102[b] × 20 000/1000 = 2040	(67[c] × 214)/1000 = 14	0.7 %

[a] Refer to Table 1.
[b] Element concentrations at the river end. Refer to Fig. 3.
[c] Averaged element concentrations in the North Branch. Refer to Figs. 4 and 5.

BGD
12, 6405–6443, 2015

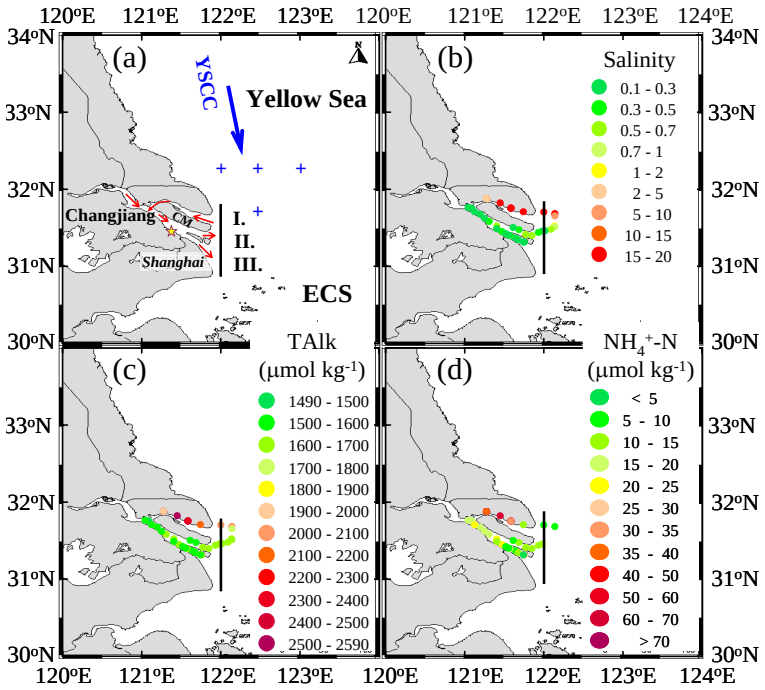

Figure 1. Area map **(a)** and surface distributions of salinity, total alkalinity and ammonia during the April 2010 cruise **(b–d)**. Following Zhai et al. (2007), we regarded the line of 122° E as the boundary between inner sub-estuaries and the outer estuary area. ECS = East China Sea; CM = Chong-ming Island; YSCC = Yellow Sea Coastal Current. As sketched in **(a)**, the inner Changjiang Estuary is geographically divided into three sub-estuaries by the Chong-ming Island and several sandbanks, i.e. the North Branch (I), the north channel of the South Branch (II), and the south channel of the South Branch (III). Four neighboring sampling sites in April 2007 (Zhai et al., 2014) were sketched in **(a)** by "+" symbols. The pentacle shows a reference station for the tidal cycle.

BGD
12, 6405–6443, 2015

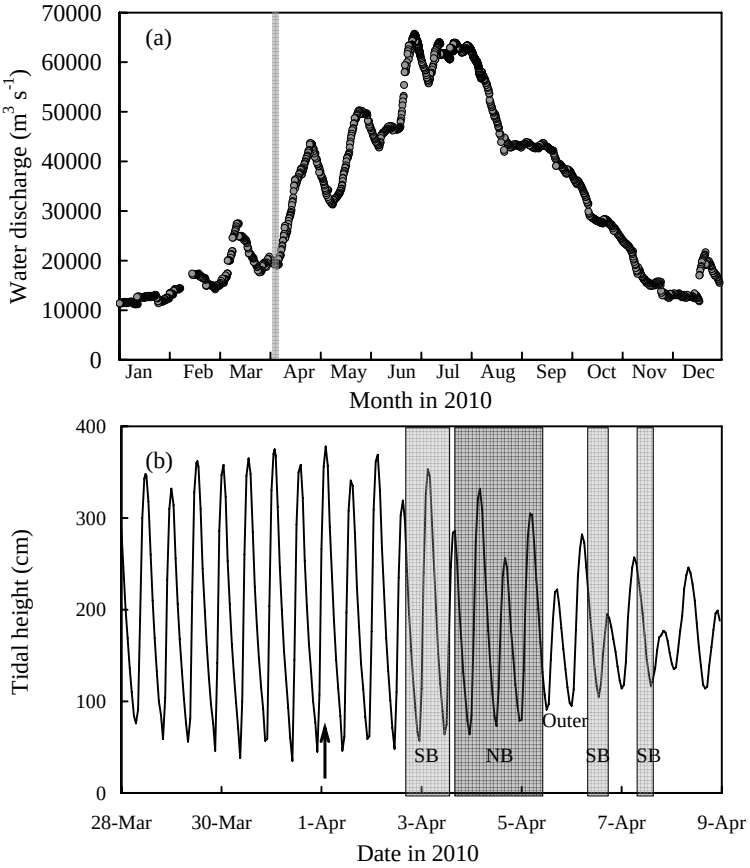

Figure 2. Water discharges from the Changjiang River **(a)** and the tidal cycles **(b)**. Grey bars represent survey periods. The arrow denotes the highest tide time in 1 April, i.e. the spring-tide day. The reference station for the tidal cycle was at 31°27′42″ N and 121°24′42″ E, as sketched in Fig. 1a. SB denotes our South Branch surveys, while NB shows the North Branch survey. "Outer" means our outer estuary survey east to 122° E.

BGD
12, 6405–6443, 2015

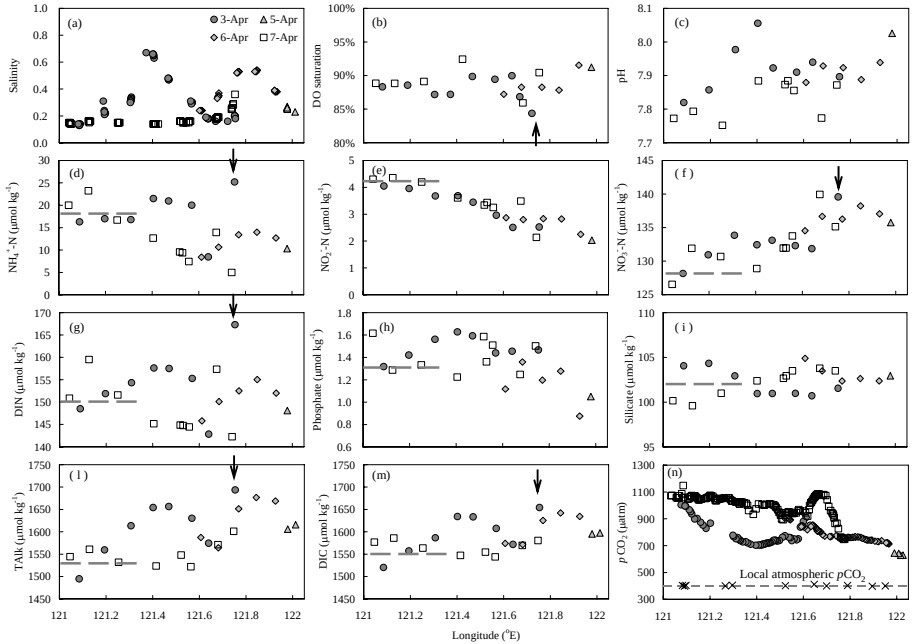

Figure 3. Evolution of surface water hydrochemical parameters in the South Branch of the inner Changjaing Estuary in early April 2010, with arrows showing signals likely from a sewage outlet, as noticed by Chai et al. (2006). Dashed lines in **(d–m)** indicate the assumed element concentrations at the river end.

BGD
12, 6405–6443, 2015

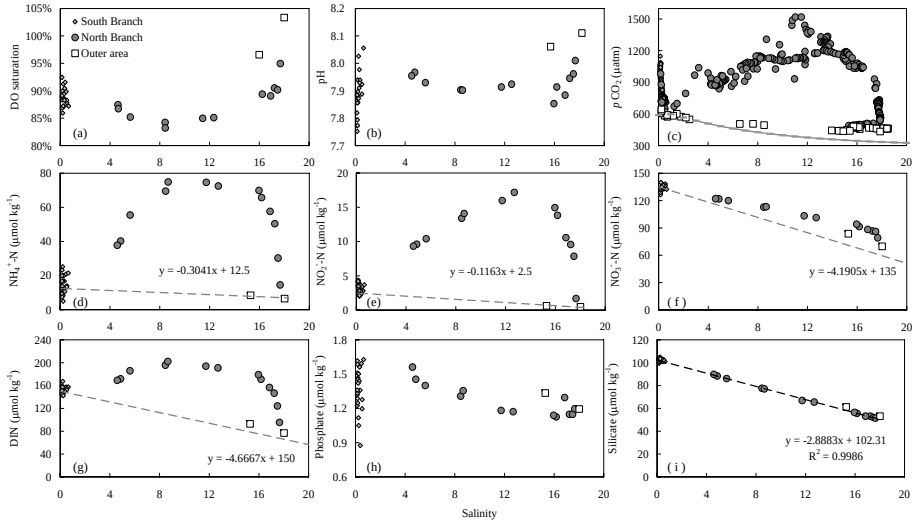

Figure 4. Surface water distributions of dissolved oxygen, pH, partial pressure of CO_2, and dissolved inorganic nutrients against salinity during the survey. Grey line in **(c)** is calculated based on conservative mixing lines of TAlk, DIC, and silicate.

BGD
12, 6405–6443, 2015

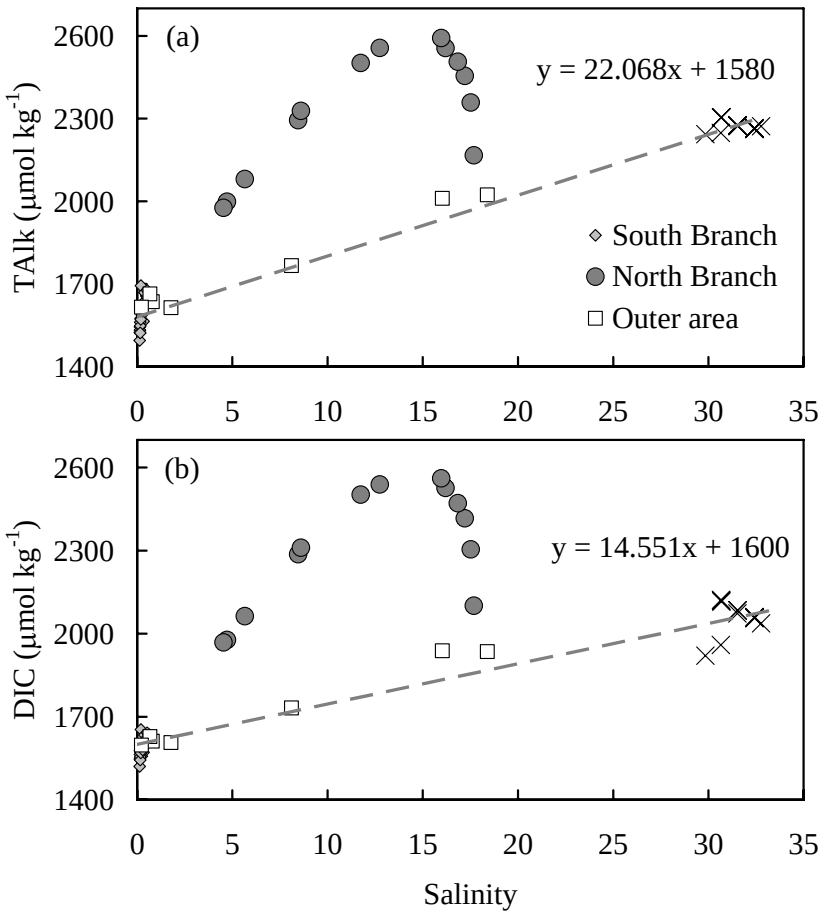

Figure 5. Surface water distributions of total alkalinity and dissolved inorganic carbon against salinity during the survey. Several April 2007 data obtained in several neighboring sites (Fig. 1a) by Zhai et al. (2014) were sketched by crossover symbols.

BGD
12, 6405–6443, 2015

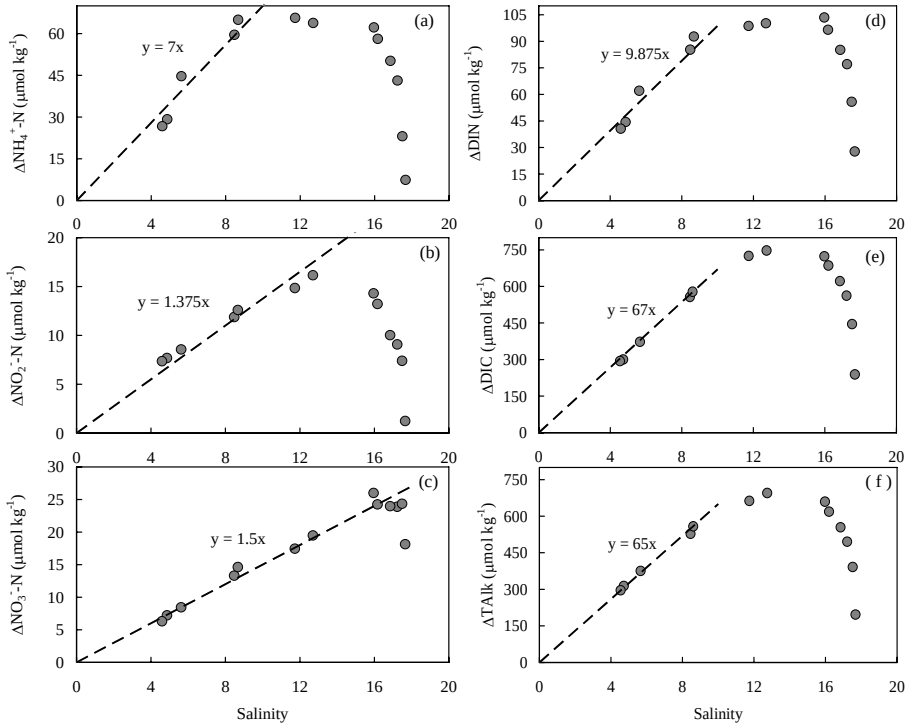

Figure 6. Biogeochemical additions of dissolved inorganic nitrogen species and carbonate system parameters against salinity in the North Branch.

BGD
12, 6405–6443, 2015

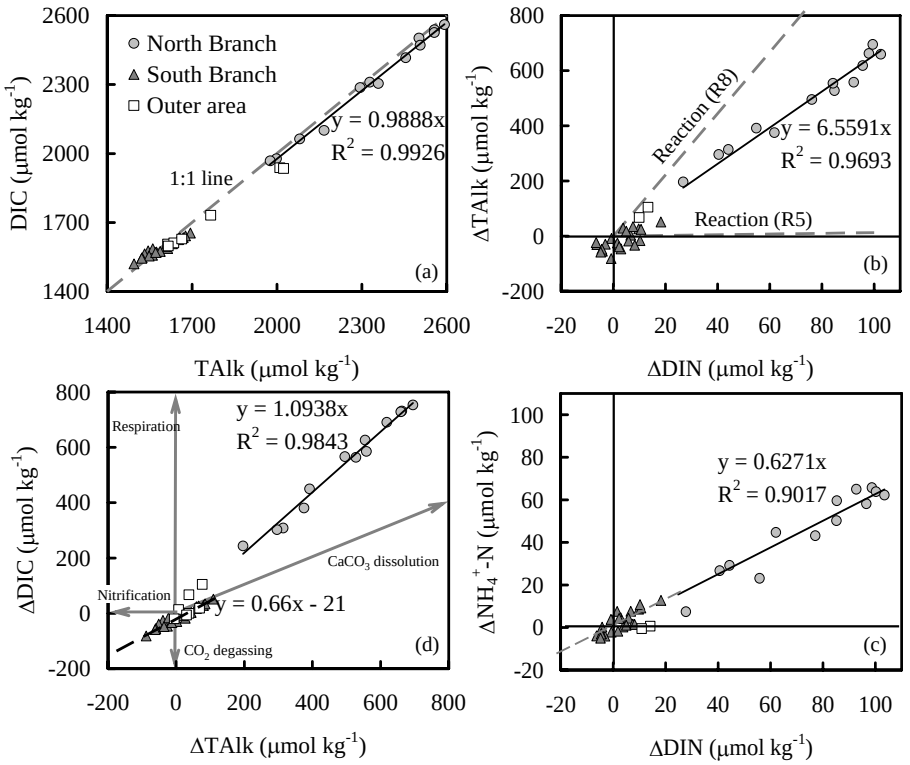

Figure 7. DIC vs. TAlk **(a)**, ΔTAlk vs. ΔDIN **(b)**, ΔNH_4^+–N vs. ΔDIN **(c)**, and ΔDIC vs. ΔTAlk **(d)**.

BGD
12, 6405–6443, 2015

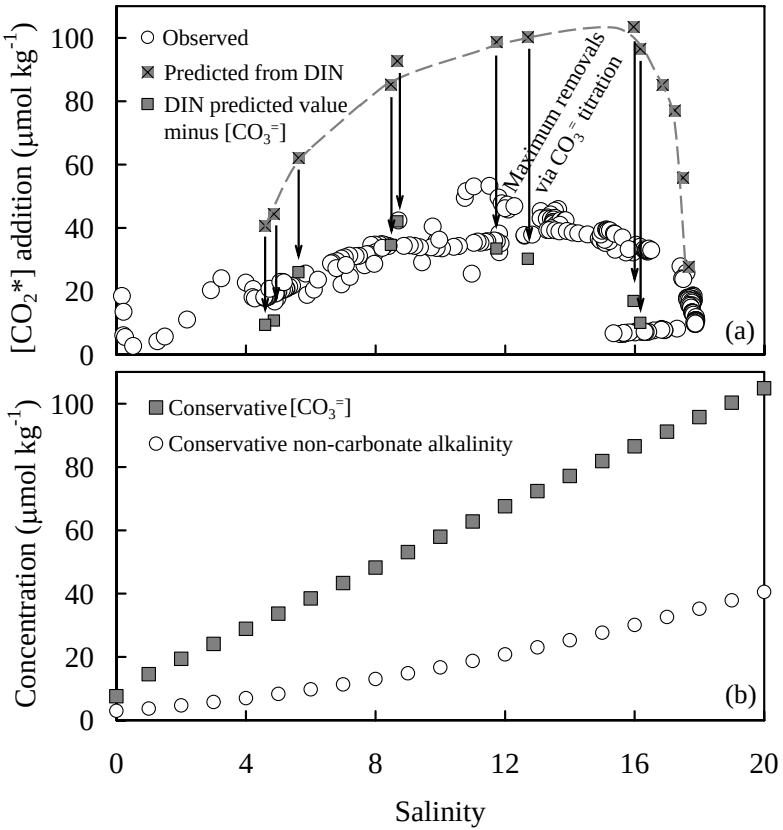

Figure 8. A comparison between field-measured $[CO_2^*]^{addition}$ and the predicted values **(a)** and the modeled conservative concentrations of CO_3^{2-} ion and non-carbonate alkalinity **(b)**. In **(a)**, conservative $[CO_3^{2-}]$ concentrations were regarded as the maximum removals of earlier free CO_2 productions. In **(b)**, non-carbonate alkalinity was defined here via (TAlk – $[HCO_3^-]$ – 2$[CO_3^{2-}]$), where $[HCO_3^-]$ and $[CO_3^{2-}]$ were calculated via DIC and TAlk data.

BGD
12, 6405–6443, 2015

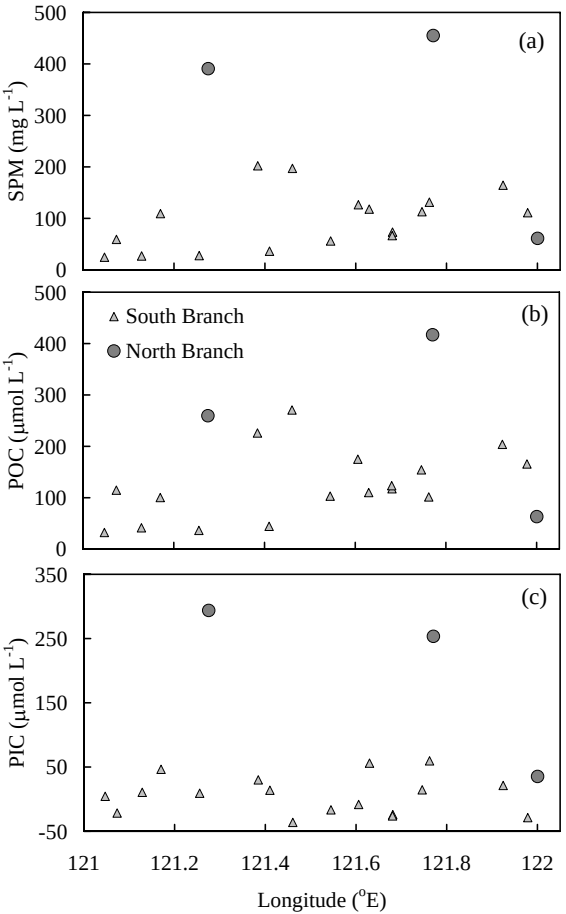

Figure A1. Surface water concentrations of suspended particulate matter **(a)**, particulate organic carbon **(b)**, and particulate inorganic carbon **(c)** in the inner Changjiang Estuary in early April 2010.

BGD
12, 6405–6443, 2015

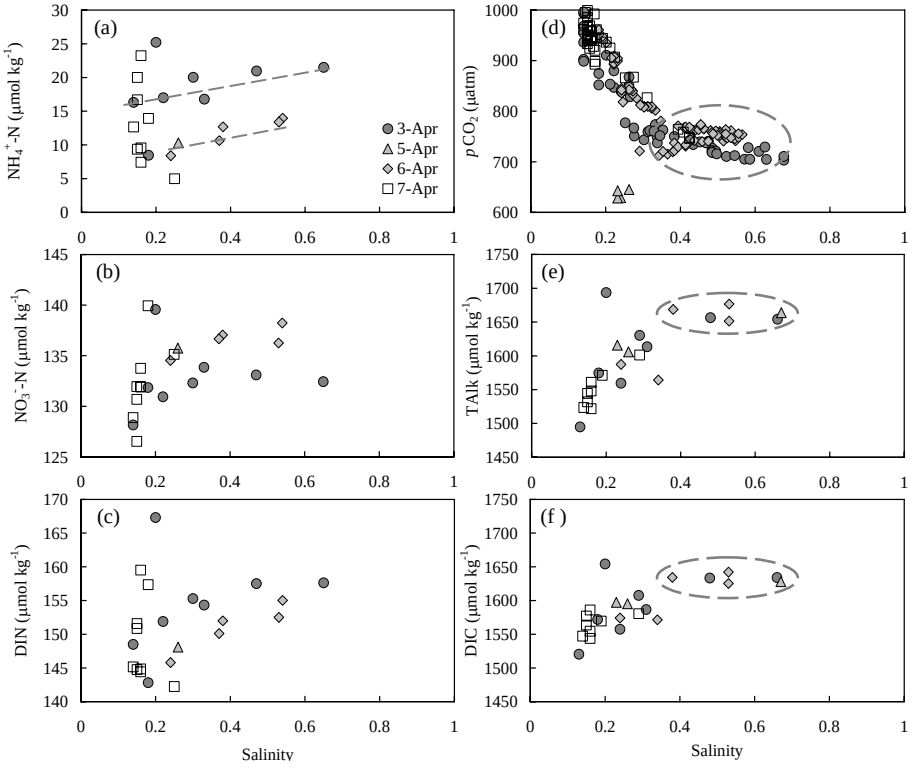

Figure A2. Surface water distributions of ammonium, nitrate, dissolved inorganic nitrogen, partial pressure of CO_2, total alkalinity, and dissolved inorganic carbon against salinity in the South Branch of the inner Changjaing Estuary in early April 2010.

BGD
12, 6405–6443, 2015